JOURNAL OF APPLIED PHYSICS **102**, 064503 (2007)

# Characterization of nitrogen-doped $Sb_2Te_3$ films and their application to phase-change memory

You Yin, Hayato Sone, and Sumio Hosaka
*Department of Nano-Material Systems, Graduate School of Engineering, Gunma University, 1-5-1 Tenjin, Kiryu, Gunma 376-8515, Japan*

(Received 28 March 2007; accepted 23 July 2007; published online 17 September 2007)

In this study, sputtered undoped and nitrogen doped $Sb_2Te_3$ (ST and STN) films were systematically investigated by x-ray diffraction (XRD) and resistance measurements. Their application to lateral phase-change memory (PCM) is presented as well. The STN film sputtered at a flow rate ratio ($N_2/Ar$) of 0.07 proved to have both high stability and low power consumption, implying its high performance in PCM applications. In the STN films ($N_2/Ar > 0.15$), the hexagonal Te phase first appeared at 160 °C, and then the orthorhombic SbN phase appeared at 290 °C. The phase separation made it very difficult for these films to switch reversibly between the crystalline and the amorphous phase. © *2007 American Institute of Physics*. [DOI: 10.1063/1.2778737]

## I. INTRODUCTION

The demand for mobile applications such as palmtops, mobile PCs, and digital cameras requires the creation of prospective nonvolatile memory (NVM) with ever higher speed, higher capacity, lower cost, lower power consumption, and so on.[1] NVM is the memory that can retain the stored information even when not powered. Flash memory, as the current NVM mainstream, can meet these requirements in the short run. However, it has many demerits, such as long write/erase time, low endurance, high programming energy, high voltage, and limited scalability beyond the 45 nm technology node by tunnel oxide.[1–3] In order to improve the performance and scalability of flash memory, several innovative concepts for alternative NVM, such as ferroelectric memory (FeRAM), magnetoresistive memory (MRAM), phase-change memory (PCM), and so on, have been put forward in the past few years.

Among these emerging NVMs, chalcogenide-based PCM is widely regarded as the most promising due to its almost perfect properties, such as excellent endurance, nondestructive reading, direct overwriting, low programming energy, huge read dynamic range, fast speed, high performance, good complementary metal-oxide-semiconductor (CMOS) logic compatibility, multistate storage.[1–4] The active chalcogenide layer in PCM is characterized by a fast reversible switching between the amorphous and the crystalline phase, accompanied by significant differences in electrical properties.[5] Chalcogenide in PCM can be amorphized via melting and quenching by applying a short but high electrical pulse so that the PCM enters a highly resistive state. On the other hand, it can be polycrystallized by applying a long but low electrical pulse, which induces the PCM to correspondingly enter a low resistive state.[6,7]

Compared with the other chalcogenides on a pseudobinary GeTe-$Sb_2Te_3$ such as the widely researched $Ge_2Sb_2Te_5$,[2–4] $Sb_2Te_3$ has been widely used in rewritable optical media[8,9] and PCM (Ref. 10) due to its fast crystallization speed and low power, both of which are made possible by its low melting point, as illustrated in Fig. 1. Nevertheless, the crystallization temperature of $Sb_2Te_3$ (<100 °C) is too low for it to be practically useful. Doping $Ge_2Sb_2Te_5$ with other elements such as Sn,[11] Ag,[12] N,[7,13,14] O,[15] greatly improves its material properties, increasing its stability and lowering the power consumption of PCM. Doping with N, among these doping elements, seems to be the most promising way to improve the physical properties. Therefore, the nitrogen doping of $Sb_2Te_3$ is expected to be an effective approach to the improvement of stability (retention time), because it increases the crystallization temperature while retaining other advantages of $Sb_2Te_3$ films. Furthermore, some proposals, such as a stacked multilayer vertical PCM structure, have been put forward recently to increase the memory capacity[16,17] or lower the power consumption[18,19] of PCM. Lateral PCMs exhibit advantages such as low RESET current and low power consumption.[20–22]

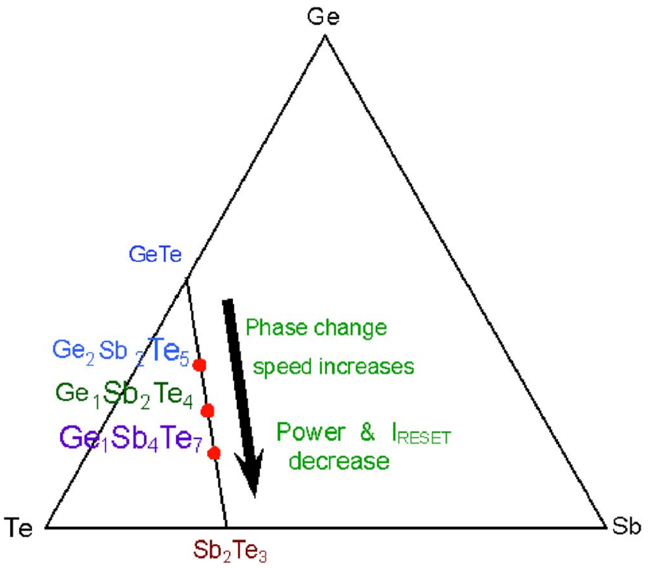

FIG. 1. Ge-Sb-Te ternary alloy phase diagram. $Sb_2Te_3$ tends to have a fast crystallization speed and low power along the GeTe-$Sb_2Te_3$ pseudobinary line.

© 2007 American Institute of Physics

Downloaded 17 Jun 2010 to 130.34.208.214. Redistribution subject to AIP license or copyright; see http://jap.aip.org/jap/copyright.jsp

TABLE I. Preparation conditions of the ST and STN films examined in this study.

| Materials | Flow rate of $N_2$ (sccm) | Flow rate of Ar (sccm) | Flow rate ratio of $N_2/Ar$ |
|---|---|---|---|
| ST | 0 | 15 | 0 |
| STN0.5 | 0.5 | 14.5 | 0.03 |
| STN1 | 1 | 14 | 0.07 |
| STN2 | 2 | 13 | 0.15 |
| STN5 | 5 | 10 | 0.5 |
| STN10 | 10 | 5 | 2 |

TABLE II. Plane indexes of the face-centered cubic (fcc) crystal structure of $Sb_2Te_3$ based on the XRD patterns of $Sb_2Te_3$ films annealed at 160 °C. Lattice constant: $a = 0.6068$ nm.

| $2\theta$ | Mea. $d$ | $h$ | $k$ | $l$ |
|---|---|---|---|---|
| 25.54 | 0.34876 | 1 | 1 | 1 |
| 29.16 | 0.30624 | 2 | 0 | 0 |
| 42.1 | 0.21463 | 2 | 2 | 0 |
| 49.68 | 0.18351 | 3 | 1 | 1 |
| 52.4 | 0.17461 | 2 | 2 | 2 |
| 61.22 | 0.1514 | 4 | 0 | 0 |
| 69.5 | 0.13525 | 4 | 2 | 0 |
| 76.96 | 0.12389 | 4 | 2 | 2 |

In this article, we present a systematic study, carried out by x-ray diffraction (XRD) and resistance measurements, of sputtered undoped and nitrogen-doped $Sb_2Te_3$ (ST and STN) films and their application in STN-based lateral phase-change memory (PCM).

## II. EXPERIMENTAL METHODS

A series of 200 nm thick ST and STN film samples with a thick $SiO_2$ capping layer on a glass substrate was prepared by changing the flow rate ratio of $N_2/Ar$ during sputtering, as given in Table I, using radio-frequency sputtering equipment (MNS-3000-RF, ULVAC, Inc.) at a background pressure below $5 \times 10^{-5}$ Pa, a sputtering pressure of 0.2 Pa and a power of 100 W. The crystal structures of these films were characterized by means of an x-ray diffractometer (RINT 2000, Rigaku Co.) after the films were annealed on a hot plate from 90 to 290 °C for 5 min. The resistivity, as a function of the annealing temperature of the films annealed in the same way, was measured using square-shaped film samples defined by Ti electrodes.

The current-voltage $(I-V)$ characteristics of the device samples were measured by a semiconductor parameter analyzer (4155B, Agilent Technologies, Ltd.). A wave form generator (Model 2571, Tabor Electronics, Ltd.) was used to apply single pulses to the devices.

## III. RESULTS AND DISCUSSION

### A. Crystal structures of ST and STN films

Figures 2(a)–2(c) show the XRD patterns of ST, STN1, and STN2 films, respectively. A number of peaks are observed in the as-deposited ST film, as shown in Fig. 1(a), which indicates that the ST film crystallized during sputtering. This is in good agreement with the fact that the crystallization temperature of ST film is below 100 °C.[23] These peaks in the XRD patterns remained below 220 °C. Based on these peak positions, the ST film was identified as a face-centered cubic (fcc) crystal structure. The plane indexes corresponding to the peak positions of the XRD patterns of the ST film annealed at 160 °C are given in Table II, and the lattice constant $a$ was found to be 0.6068 nm. It is interesting that the peaks in the patterns generally tended to shift to a larger angle with increasing annealing temperature up to 160 °C. Correspondingly, the movement of the peaks re-

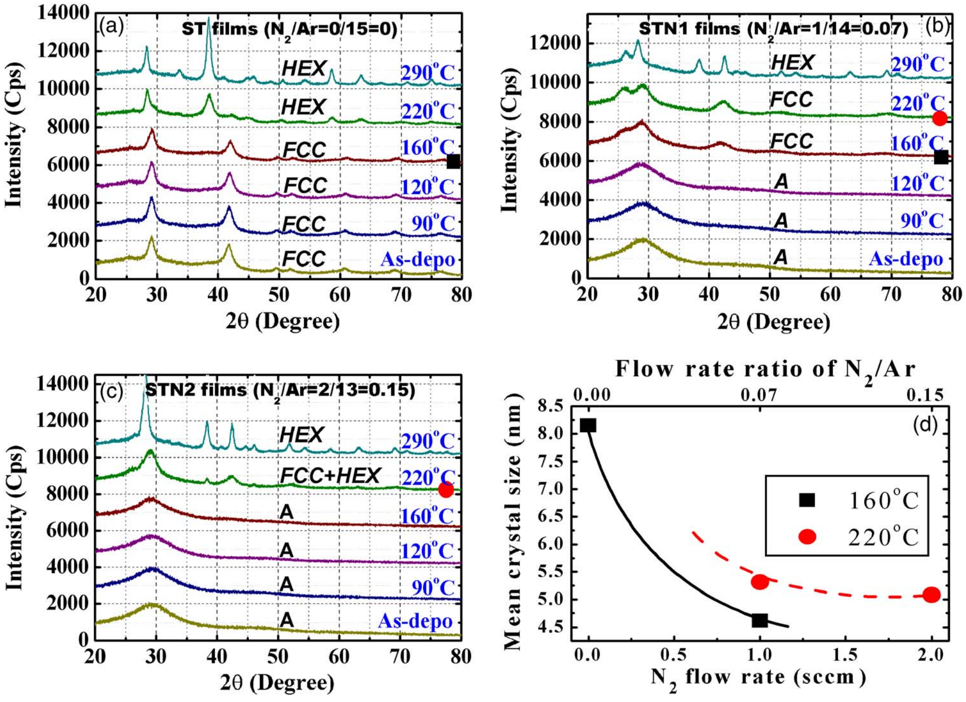

FIG. 2. XRD patterns of (a) ST, (b) STN1, and (c) STN2. (d) Mean crystal size as a function of the $N_2$ flow rate.

Downloaded 17 Jun 2010 to 130.34.208.214. Redistribution subject to AIP license or copyright; see http://jap.aip.org/jap/copyright.jsp

TABLE III. Plane indexes of the hexagonal crystal structure of $Sb_2Te_3$ based on the XRD patterns of $Sb_2Te_3$ films annealed at 290 °C. Lattice constants: $a=0.4262$ nm, $c=3.045$ nm.

| $2\theta$ | Mea. $d$ | $h$ | $k$ | $l$ |
|---|---|---|---|---|
| 26.3 | 0.33886 | 0 | 0 | 9 |
| 28.3 | 0.31535 | 0 | 1 | 5 |
| 33.62 | 0.26656 | 0 | 1 | 8 |
| 38.44 | 0.23418 | 1 | 0 | 10 |
| 40.9 | 0.22064 | 0 | 1 | 11 |
| 44.6 | 0.20316 | 0 | 0 | 15 |
| 45.94 | 0.19754 | 1 | 0 | 13 |
| 48.58 | 0.1874 | 0 | 1 | 14 |
| 50.6 | 0.18039 | 1 | 1 | 9 |
| 54.22 | 0.16917 | 0 | 0 | 18 |
| 58.6 | 0.15753 | 0 | 2 | 10 |
| 63.4 | 0.14671 | 1 | 0 | 19 |
| 66.56 | 0.14049 | 0 | 1 | 20 |
| 69.14 | 0.13586 | 1 | 2 | 5 |
| 70.96 | 0.13282 | 0 | 2 | 16 |
| 74.9 | 0.12678 | 2 | 1 | 10 |
| 76.52 | 0.12449 | 0 | 1 | 23 |

sulted in the reduction of the lattice constant, demonstrating that the ST film became more ordered (e.g., reduction in grain boundary via grain growth) with increasing annealing temperature. The appearance of a pattern at 220 °C implies that a phase transformation of the ST films from fcc to the other phase occurred between 160 and 220 °C. The phase was identified as a hexagonal crystal structure according to the XRD patterns at 290 °C (Table III). The lattice constants $a$ and $c$ were found to be 0.4262 and 3.045 nm, respectively. A very broad peak at around 29° ($2\theta$) was observed for the as-deposited STN1 and STN2 films, as shown in Figs. 2(b) and 2(c), which indicates that these two films were amorphous. The fcc XRD pattern of STN1 appeared at 160 °C and 220 °C. The crystal structures of both STN1 and STN2 were hexagonal at 290 °C. Both fcc and hexagonal peaks were also observed for STN2 at 220 °C. The mean crystal sizes of the films at the same temperatures of 160 °C and 220 °C were estimated using Scherrer's equation[24,25] and are summarized in Fig. 2(d). As we can see, the crystal size could be effectively refined by increasing the $N_2$ flow rate during sputtering. This is in good agreement with the refinement of the crystal size in the case of the N doping of $Ge_2Sb_2Te_5$.[26]

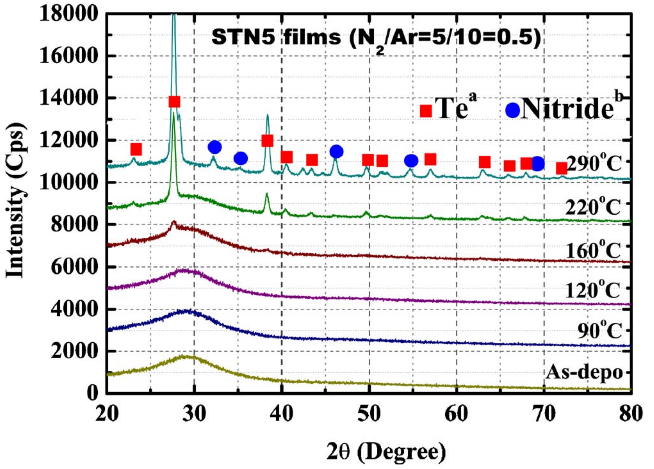

FIG. 3. XRD patterns of STN5. The hexagonal Te phase appears first at 160 °C, followed by the orthorhombic SbN phase at 290 °C.

It is very interesting that the further increase of the $N_2$ flow rate during sputtering led to a set of very different patterns, as shown in Fig. 3. The STN5 film was amorphous up to 120 °C. The STN5 film annealed at 290 °C was found to be composed of hexagonal Te ($a=0.445$ nm; $c=0.59$ nm) and orthorhombic SbN ($a=0.492$ nm; $b=1.246$ nm; $c=0.542$ nm). The peaks of Te and SbN are marked as solid squares and circles in Fig. 3, respectively, and given in Table IV. When comparing the peaks in the XRD patterns for 160 °C and 220 °C with those for 290 °C, it can be readily concluded that Te crystallites first formed at a temperature of around 160 °C and SbN nitride at a high annealing temperature (e.g., 290 °C). The typical XRD patterns of STN5 shown here are similar to those observed for STN10 (data not shown).

The phases and crystal structures of the ST and STN films are summarized in Table V. On the whole, the temperature of crystallization to fcc increased with increasing $N_2$ flow rate at a low flow rate ratio. In this case, the nitrogen atoms in the film can be located at the interstitial sites in the fcc or in the hexagonal lattices of chalcogenides.[26] The fcc phase of STN1 had the widest temperature window among the STN films, which is advantageous for PCM applications. This is because, as is well known, a fast reversible phase transformation between the fcc and the amorphous phase is usually needed for memory storage.[27–29] An excessively high $N_2$ flow rate can result in the phase separation of Te and

TABLE IV. Plane indexes of the crystal structures based on the XRD patterns of the STN5 ($N_2$/Ar=5/10) film annealed at 290 °C. The film is composed of hexagonal Te ($a=0.445$ nm and $c=0.59$ nm) and orthorhombic SbN ($a=0.492$ nm, $b=1.246$ nm, and $c=0.542$ nm).

| $2\theta$ | Mea. $d$ | $h$ | $k$ | $l$ |
|---|---|---|---|---|
| 23.1[a] | 0.38502 | 1 | 0 | 0 |
| 27.64[a] | 0.32272 | 1 | 0 | 1 |
| 32.2[b] | 0.27799 | 1 | 3 | 1 |
| 35.16[b] | 0.25523 | 0 | 2 | 2 |
| 38.4[a] | 0.23441 | 1 | 0 | 2 |
| 40.52[a] | 0.22262 | 1 | 1 | 0 |
| 43.4[a] | 0.20849 | 1 | 1 | 1 |
| 46.14[b] | 0.19673 | 2 | 3 | 1 |
| 49.74[a] | 0.1833 | 2 | 0 | 1 |
| 51.38[a] | 0.17783 | 1 | 1 | 2 |
| 54.68[b] | 0.16785 | 1 | 1 | 3 |
| 57.06[a] | 0.1614 | 2 | 0 | 2 |
| 62.98[a] | 0.14758 | 1 | 1 | 3 |
| 63.9[a] | 0.14568 | 2 | 1 | 0 |
| 65.98[a] | 0.14158 | 2 | 1 | 1 |
| 67.96[a] | 0.13793 | 1 | 0 | 4 |
| 69.12[b] | 0.1359 | 0 | 0 | 4 |
| 72.18[a] | 0.13087 | 2 | 1 | 2 |

[a] Hexagonal Te.

[b] Orthorhombic SbN.

Downloaded 17 Jun 2010 to 130.34.208.214. Redistribution subject to AIP license or copyright; see http://jap.aip.org/jap/copyright.jsp

TABLE V. Phases of ST and STN films as determined from the XRD patterns.

| Material | As-depo | 160 °C | 220 °C | 290 °C |
|---|---|---|---|---|
| ST | fcc ST | fcc ST | hexagonal ST | hexagonal ST |
| STN1 | amorphous STN | fcc STN | fcc STN | hexagonal STN |
| STN2 | amorphous STN | amorphous STN | fcc STN+hexagonal STN | hexagonal STN |
| STN5 | amorphous STN | hexagonal Te | hexagonal Te | hexagonal Te+orthorhombic SbN |

SbN, which is very harmful to reversible phase change. From the above analysis, it is considered that STN films are preferable for PCM applications when the $N_2$ flow rate is around 1 sccm, due to their wide fcc temperature range and high crystallization temperature. The reversibility (or cyclability of PCM) and stability (long retention time) can be greatly improved by adopting STN1 film ($N_2/Ar=0.07$) as a PCM medium.

### B. Temperature dependence of the resistivity

Figure 4 shows the resistivities of ST and STN films as a function of the annealing temperature up to 300 °C. It has been reported that the thicknesses of Te-based phase-change materials were reduced by 5%–10% as a result of phase change.[30] Nevertheless, it is reasonable to assume that the influence of the film thickness reduction on the resistivity can be ignored here. The resistivity of the as-deposited ST film was around $9\times10^{-2}$ Ω cm, because the as-deposited ST film was already crystalline. The resistivity of the ST film decreased in the temperature range of 100 °C–300 °C. The reason for the resistivity reduction is that the fcc crystals became larger and more ordered (see the discussion in Sec. III A) and a phase transformation from fcc to a hexagonal structure took place [see the XRD patterns in Fig. 2(a)]. The resistivity of the as-deposited amorphous STN film, however, was around 100–1000 times of that of the ST film. Crystallization to fcc led to the marked reduction in resistivity of the STN1 film, from around $9\times10^{1}$ Ω cm to around $8\times10^{-3}$ Ω cm, that is, by about 4 orders of magnitude. The phase transformation from fcc to a hexagonal structure resulted in a further resistivity drop to around $4\times10^{-3}$ Ω cm at 300 °C. The increase in the resistivity of the STN2 film might be due to the formation of SbN nitride, which is so small that it was almost undetectable by XRD.

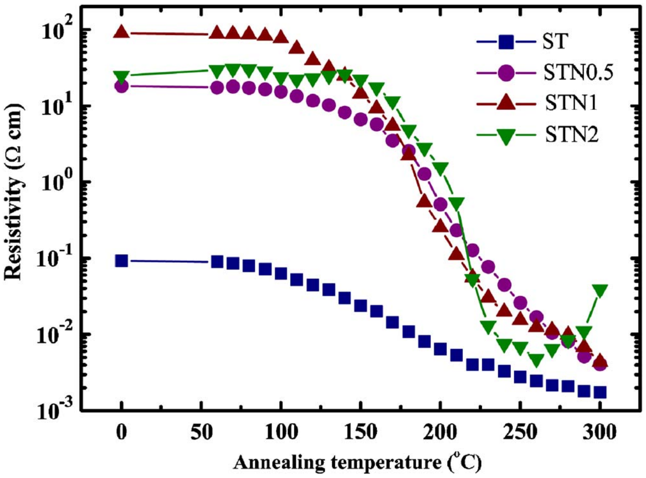

FIG. 4. Resistivities of ST and STN films as a function of the annealing temperature.

### C. Lateral PCM

A 150 nm thick ST or STN layer, covered by ZnS-$SiO_2$, was used in the lateral device. The gap length, *L*, between the two electrodes and the gap width, *W*, were 0.4 and 0.7 μm, respectively. The pulse-mode $R-V$ characteristics of the devices are shown in Fig. 5. The pulse width, $t_{RESET}$, was 20 ns. The resistance of the ST, STN1, and STN2 devices dramatically increased by two or three orders of magnitude at a RESET voltage ($V_{RESET}$) of around 9.5 V, 7 V, and 6.5 V, respectively. The required dissipated energy ($E_{RESET}$) for the RESET operation was estimated using the equation $(V_{RESET}^2/R_{SET})\times t_{RESET}$. The required $E_{RESET}$ energies of the ST, STN1, and STN2 devices were calculated to be around $6\times10^{-10}$ J, $3.3\times10^{-9}$ J, and $2.8\times10^{-9}$ J. From the view-

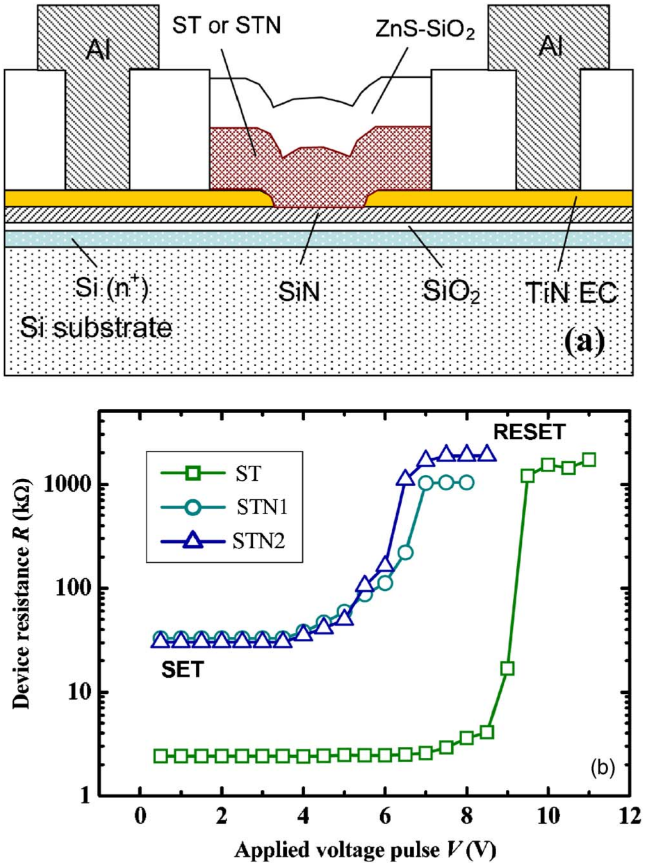

FIG. 5. (a) Schematic of lateral single-layer PCM devices. (b) Pulse-mode $R-V$ characteristics of the devices.

Downloaded 17 Jun 2010 to 130.34.208.214. Redistribution subject to AIP license or copyright; see http://jap.aip.org/jap/copyright.jsp

point of power consumption as well, STN1 film may be the preferable medium for PCM applications rather than ST film.

## IV. CONCLUSIONS

We have investigated ST and STN films by means of XRD and resistivity measurements, as well as possible PCM applications of the films. Based on these experiments, some conclusions can be drawn, as follows.

(1) STN1 film ($N_2/Ar=0.07$) is preferable in PCM applications because of the stability of both the amorphous and the fcc phase, which is due to its high crystallization temperature and wide fcc temperature range.
(2) For the STN films sputtered at a high flow rate ratio of $N_2/Ar$ ($>0.15$), the hexagonal Te phase appears first at 160 °C, followed by the orthorhombic SbN phase at 290 °C. Phase separation is very harmful to the reversibility of PCM in these films.
(3) From the viewpoint of power consumption as well, STN1 film is the preferable medium for PCM applications.

## ACKNOWLEDGMENTS

We would like to acknowledge the financial support of the Semiconductor Technology Academic Research Center (STARC) of Japan, and the help given to us by Professor Furusawa for the XRD experiments and by Mr. Higano for the resistivity measurements, both from the Gunma University, Japan.

[1] R. Bez and A. Pirovano, Mater. Sci. Semicond. Process. **7**, 349 (2004).
[2] S. Lai, Tech. Dig. - Int. Electron Devices Meet. **2003**, 255 (2003).
[3] Y. Yin, A. Miyachi, D. Niida, H. Sone, and S. Hosaka, Jpn. J. Appl. Phys., Part 1 **45**, 3238 (2006).
[4] S. Lai and T. Lowrey, Tech. Dig. - Int. Electron Devices Meet. **2001**, 803 (2001).
[5] S. R. Ovshinsky, Phys. Rev. Lett. **21**, 1450 (1968).
[6] Y. Yin, H. Sone, and S. Hosaka, Jpn. J. Appl. Phys., Part 1 **45**, 6177 (2006).
[7] Y. Yin, H. Sone, and S. Hosaka, Jpn. J. Appl. Phys., Part 1 **45**, 8600 (2006).
[8] M. H. R. Lankhorst, L. V. Pieterson, and M. V. Schijndel, Jpn. J. Appl. Phys., Part 1 **42**, 863 (2003).
[9] N. Yamada, E. Ohno, K. Nishiuchi, N. Akahira, and M. Takao, J. Appl. Phys. **69**, 2849 (1991).
[10] B. Liu, Z. Song, S. Feng, and B. Chen, Microelectron. Eng. **82**, 168 (2005).
[11] T. J. Park, D. H. Kim, S. M. Yoon, K. J. Choi, N. Y. Lee, B. G. Yu, and S. Y. Choi, Jpn. J. Appl. Phys., Part 1 **45**, L1273 (2006).
[12] C. T. Lie, P. C. Kuo, W. C. Hsu, T. H. Wu, P. W. Chen, and S. C. Chen, Jpn. J. Appl. Phys., Part 1 **42**, 1026 (2003).
[13] R. Kojima, S. Okabayashi, T. Kashihara, K. Horai, T. Matsunaga, E. Ohno, N. Yamada, and T. Ohta, Jpn. J. Appl. Phys., Part 1 **37**, 2098 (1998).
[14] H. Horii, J. H. Park, J. H. Yi, B. J. Kuh, and Y. H. Ha, IEICE Trans. Electron. **87-C**, 1673 (2004).
[15] L. Men, J. Tominaga, H. Fuji, and N. Atoda, Jpn. J. Appl. Phys., Part 1 **39**, 2639 (2000).
[16] Y. F. Lai and Y. Y. Lin, T. A. Tang, B. C. Cai, and B. Chen, Appl. Phys. A **84**, 21 (2006).
[17] F. Rao, Z. Song, M. Zhong, L. Wu, G. Feng, B. Liu, S. Feng, and B. Chen, Jpn. J. Appl. Phys., Part 1 **46**, L25 (2007).
[18] T. C. Chong, L. P. Shi, R. Zhao, P. K. Tan, J. M. Li, H. K. Lee, and X. S. Miao, Appl. Phys. Lett. **88**, 122114 (2006).
[19] K. A. Campbell and C. M. Anderson, Microelectron. J. **38**, 52 (2007).
[20] Y. Yin, A. Miyachi, D. Niida, H. Sone, and S. Hosaka, Jpn. J. Appl. Phys., Part 1 **45**, L726 (2006).
[21] M. Lankhorst, B. Ketelaars, and R. Wolters, Nat. Mater. **4**, 347 (2005).
[22] F. Merget, D. H. Kim, P. H. Bolivar, and H. Kurz, Microsyst. Technol. **13**, 169 (2006).
[23] T. L. Anderson and H. B. Krause, Acta Crystallogr., Sect. B: Struct. Crystallogr. Cryst. Chem. **30**, 1307 (1974).
[24] H. P. Klug and L. E. Alexander, *X-Ray Diffraction Procedures for Polycrystalline and Amorphous Materials* (John Wiley & Sons, New York, 1974), Chap. 9, p. 689.
[25] Y. Yin, H. Sone, and S. Hosaka, Jpn. J. Appl. Phys., Part 1 **44**, 6208 (2005).
[26] T. H. Jeong, M. R. Kim, H. Seo, J. W. Park, and C. Yeon, Jpn. J. Appl. Phys., Part 1 **39**, 2775 (2000).
[27] N. Yamada, E. Ohno, K. Nishiuchi, N. Akahira, and M. Takao, J. Appl. Phys. **69**, 2849 (1991).
[28] A. Pirovano, A. L. Lacaita, A. Benvenuti, F. Pellizzer, and R. Bez, IEEE Trans. Electron Devices **51**, 452 (2004).
[29] Z. Sun, J. Zhou, and R. Ahuja, Phys. Rev. Lett. **96**, 055507 (2006).
[30] T. P. L. Pedersen, J. Kalb, W. K. Njoroge, D. Wamwangi, M. Wuttig, and F. Spaepen, Appl. Phys. Lett. **79**, 3597 (2001).

Downloaded 17 Jun 2010 to 130.34.208.214. Redistribution subject to AIP license or copyright; see http://jap.aip.org/jap/copyright.jsp